inorganics

MDPI

Article

Enhanced Photocatalytic Activity of WS_2/TiO_2 Nanofibers for Degradation of Phenol under Visible Light Irradiation

Engy Ahmed Nada [1], Heba Hassan El-Maghrabi [2,*], Patrice Raynaud [3], Hager Rabea Ali [4], Saad Abd El-Wahab [1], Dina Yahea Sabry [1], Yasser Mohamed Moustafa [4] and Amr Ahmed Nada [4,*]

[1] Chemistry Department, Faculty of Science, Ain Shams University, Cairo 11566, Egypt; engyahmednada@gmail.com (E.A.N.); saadabdelwahab@sci.asu.edu.eg (S.A.E.-W.); d.y_sabry@yahoo.com (D.Y.S.)
[2] Department of Refining, Egyptian Petroleum Research Institute, Cairo 11727, Egypt
[3] Laboratoire Plasma et Conversion d'Energie (LAPLACE), Université de Toulouse, CNRS, INPT, UPS, 31062 Toulouse, France; raynaud@laplace.univ-tlse.fr
[4] Department of Analysis and Evaluation, Egyptian Petroleum Research Institute, Cairo 11727, Egypt; hagerchem@gmail.com (H.R.A.); ymoustafa12@yahoo.com (Y.M.M.)
* Correspondence: hebachem@yahoo.com (H.H.E.-M.); chem_amr@yahoo.com (A.A.N.)

Abstract: Binary composite WS_2/TiO_2 nanofibers (WTN) were elaborated by electrospinning technique. The photocatalytic efficiency of the binary nanofibers was changed via different ratios between WS_2 and TiO_2. The structural, morphological and optical properties of the prepared nanofibers were evaluated by Raman spectroscopy, Fourier transform infrared spectroscopy (FT-IR), scanning electron microscopy (SEM) and UV-Vis diffuse reflectance spectroscopy (UV-vis/DRS), respectively. The prepared nanofibers showed a remarkable performance in photocatalytic efficiency of phenol compound degradation under visible light. WTN nanofibers showed superior photocatalytic activity (83%) and high stability of several cycles under visible light. Therefore, WS_2/TiO_2 nanofibers have great prospects for the treatment of wastewater from toxic organic contamination due to their excellent photocatalytic performance reusability and recyclability.

Keywords: nanofibers; tungsten disulfide; TiO_2; phenol photodegradation

Citation: Nada, E.A.; El-Maghrabi, H.H.; Raynaud, P.; Ali, H.R.; Abd El-Wahab, S.; Sabry, D.Y.; Moustafa, Y.M.; Nada, A.A. Enhanced Photocatalytic Activity of WS_2/TiO_2 Nanofibers for Degradation of Phenol under Visible Light Irradiation. *Inorganics* **2022**, *10*, 54. https://doi.org/10.3390/inorganics10040054

Received: 27 February 2022
Accepted: 15 April 2022
Published: 18 April 2022

1. Introduction

The development of industries throughout the world has led to increase water contamination which implies a serious threat to humans and environment [1,2]. Water pollution is a matter of concern worldwide. Wastewater is caused by synthetic chemicals being released from a variety of anthropogenic industry sources. In particular, the petroleum refinery waste, which is one of the harmful sources for water, along with phenol compound which is one of these mischievous sources [3]. The different technologies for water treatment and purification have been extensively discussed in the literature as the design and the operation of affordable methods remains a challenge. The treatment methods include membrane separation, electrochemical method, chemical precipitation, adsorption, photocatalysis, etc. [4]. It is pertinent to highlight that all treatment methods have their own technical and economic limitations for real-life applications. However, photocatalysis technique is one important method as it prevents to form the secondary pollutants [5].

Titanium dioxide (TiO_2) is one of the most significant photocatalysts, which is extensively utilized in various fields, such as electrochemistry and photocatalysis due to its several benefits such as low cost, nontoxicity, good chemical stability and excellent oxidizing power [3]. However, it has some drawbacks such as lack of activity in the abundant visible light energy because TiO_2 generally exhibits good photocatalytic activity in near ultraviolet (UV), due to its large bandgap energy (3.2 eV) [6]. To address these issues, it has been combined with other nanomaterials to enhance its photo-adsorption capacity

under visible light such as CdS, NiO, $ZnFe_2O_4$, Ag_2CO_3, Fe_2O_3 and Fe_3O_4 [7,8]. The photocatalytic efficiency of TiO_2–NFs can be improved by metals, non-metals and semiconductors [9,10]. In addition, titanium dioxide is extensively utilized for environmental purification applications [11] and tungsten disulfide (WS_2) is one of the important materials for TiO_2 enhancement.

Tungsten disulfide (WS_2) is one of the transition-metal dichalcogenide compounds which have inherent excellent photoactivity. The bandgap of WS_2 is approximately 1.9 eV when the thickness is reduced down to monolayers, which access the absorption from visible light and utilize solar energy sufficiently [12].

In this contribution, WS_2/TiO_2 nanofibers were elaborated by combined 1D and 2D structures by electrospinning. The morphology, structure and optical properties of the nanocomposites were evaluated. The photocatalytic efficiency of WS_2/TiO_2 nanofibers for the degradation of phenol, as an organic pollutant, was estimated under the visible light illumination.

2. Results and Discussion

2.1. Characterization of TWx Nanofibers

XRD spectra of the prepared WS_2/TiO_2 nanofibers are shown in Figure 1. It is clear that the diffraction peaks of 25.5°, 38.1°, 48.1°, 54.1°, 55.3° and 62.9° are correspondent to the standard characteristic peaks position of (101), (004), (200), (105), (211) and (204) crystal planes of anatase TiO_2, respectively (JCPDS No. 01-084-1285). In addition, the peaks at 28.98°, 32.81°, 33.64°, 39.64° and 58.48° can be well indexed to the (002), (004), (100), (100), (103) and (008), respectively (JCPDS No. 01-084-1285) of WS_2 [13]. The narrow and sharp peaks suggest that the product is highly crystalline. Where, the different weight ratios of TiO_2 to WS_2 (1:0, 0.9:0.1, 0.8:0.2, 0.7:0.3, 0.6:0.4 and 0.5:0.5) to obtain (TW0, TW10, TW20, TW30, TW40 and TW50, respectively).

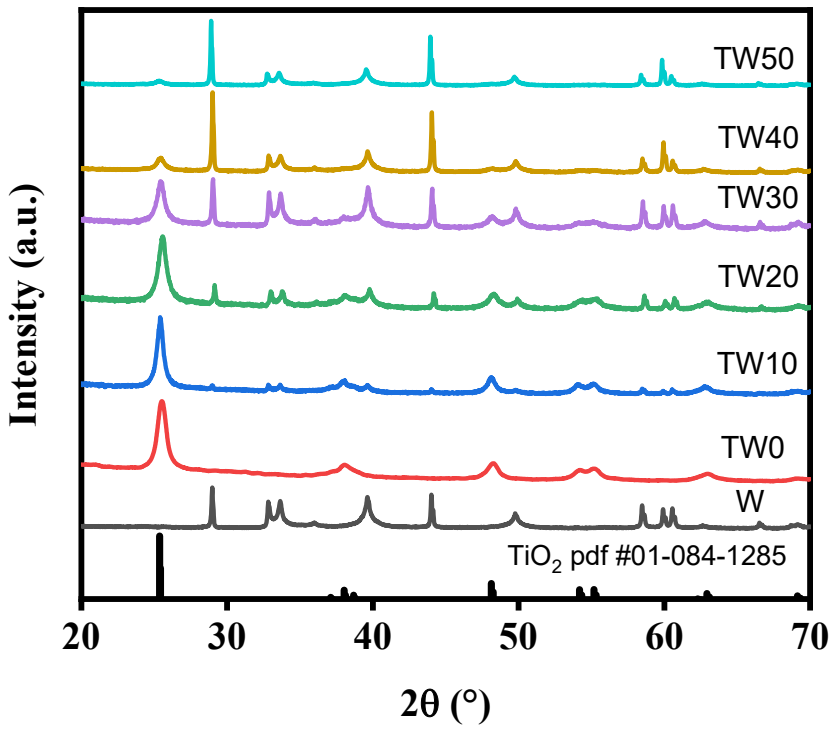

Figure 1. XRD for W, TW0, TW10, TW20, TW30, TW40 and TW50 nanofibers of TiO_2:WS_2 (0:1, 1:0, 0.9:0.1, 0.8:0.2, 0.7:0.3, 0.6:0.4 and 0.5:0.5, respectively).

The WS_2/TiO_2 nanofibers with different ratio between tungsten disulfide and titanium dioxide were observed with the use of Raman measurements. Moreover, Raman spectra of the prepared nanofibers are presented in Figure 2. In W sample, the bands at 126.28,

255.03, 320.11, 409.71, 701.09 and 799.35 cm^{-1} can be ascribed to the vibration bands of WS_2 nanosheets [14,15]. For pure TiO_2 sample, the bands observed at 147.41, 198.17, 389.58, 502.31 and 626.37 cm^{-1} in the Raman spectrum can be assigned to E^1_g, E^2_g, $B_{1g}(1)$, $B_{1g}(2)$ + A_{1g} and E^3_g modes of anatase, respectively [16]. The combination of WS_2 with TiO_2 (in TW10, TW20, TW30, TW40 and TW50) resulted in a slight change in the anatase bands. In TW40 and TW50, the main band of anatase at 150 cm^{-1} is significantly changed due to the overlapping between the bands of TiO_2 and WS_2 and it means that there is a high conjugation between TiO_2 and WS_2.

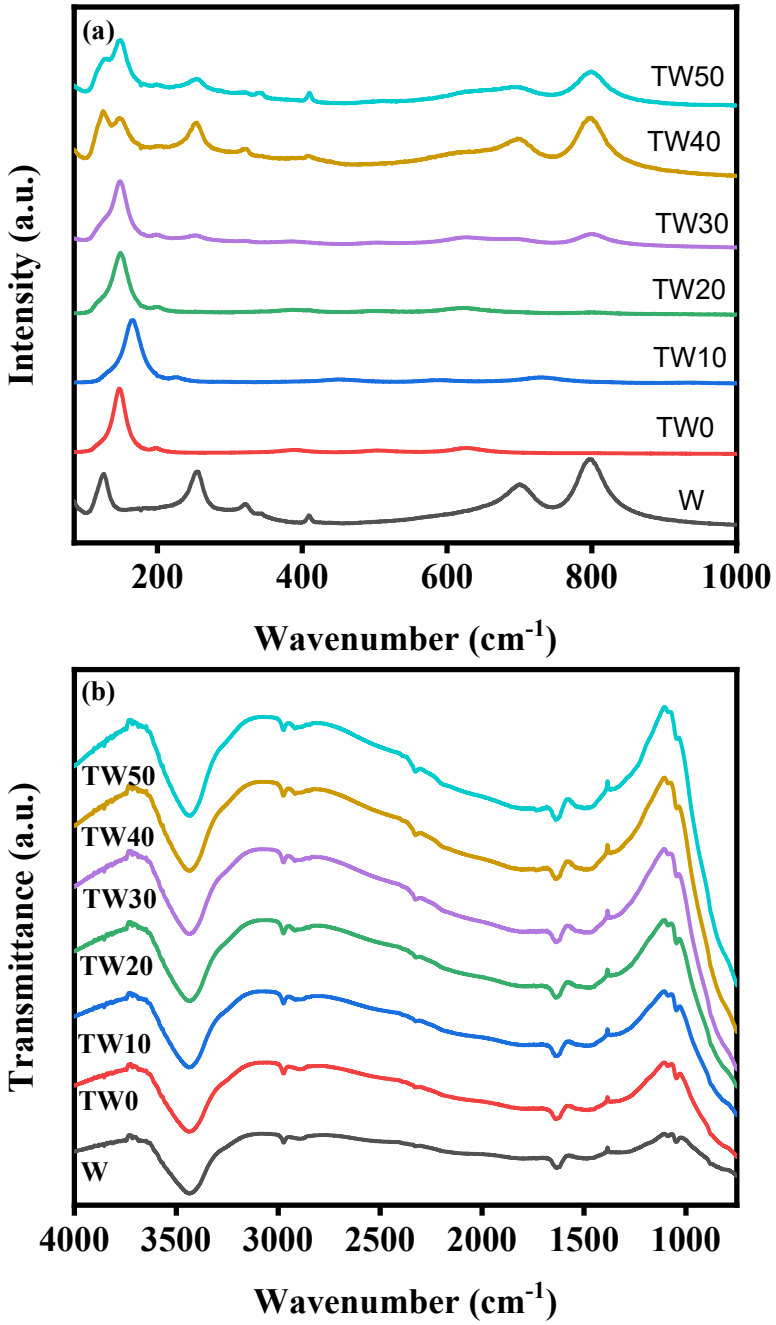

Figure 2. (**a**) Raman spectra and (**b**) FTIR for TW0, TW10, TW20, TW30, TW40 and TW50 nanofibers.

The conjugation between WS_2 and TiO_2 can also be detected by the FTIR transmission spectra presented in Figure 2b. The band located around 3450 cm^{-1} is attributed to the O–H bonds for all nanofibers [17–19]. The overlap between the peaks of Ti–O and W–S

was presented for all nanocomposite samples of TWx which confirmed the successful conjugation between TiO_2 and WS_2.

The surface area results showed that S_{BET} of TW0, TW10, TW20, TW30, TW40 and TW50 are 17, 25, 42, 61, 73 and 78 m^2/g. The surface area of (1D) TiO_2 was enhanced by interacting with the (2D) structure of WS_2. It is well known that TiO_2 with large surface area has excellent photocatalytic activity as a result of providing more active adsorption sites and speed transport channels for large organic molecules which were detected in TiO_2 with WS_2.

The morphology of fabricated nanofibers was observed using scanning electron microscope as presented in Figure 3a–f. The T, TW10, TW20, TW30, TW40 and TW50 nanofibers have 97 ± 8, 120 ± 5, 188 ± 4, 210 ± 8, 240 ± 7 and 290 ± 9 nm average diameter, respectively. The increase in the diameter of the WS_2-enriched nanofibers was attributed to the viscosity of electro-spun solution coming from WS_2, which contributed to the successful incorporation between WS_2 and TiO_2 nanofibers. These findings are consistent with those of Raman measurements. EDX mappings for TW40 are presented in Figure 3g–l. The distribution of WS_2 is uniform with TiO_2 nanofibers. AAS demonstrated that the total Ti:W atomic ratios were approximately 0.902:0.098, 0.801:0.199, 0.704:0.296, 0.602:0.398 and 0.505:0.495 in TW10, TW20, TW30, TW40 and TW50, respectively. Indicating that TiO_2 and WS_2 were uniformly distributed throughout the network structure according to the preparation designed. Their uniform distribution should contribute to their photocatalytic activity as presented.

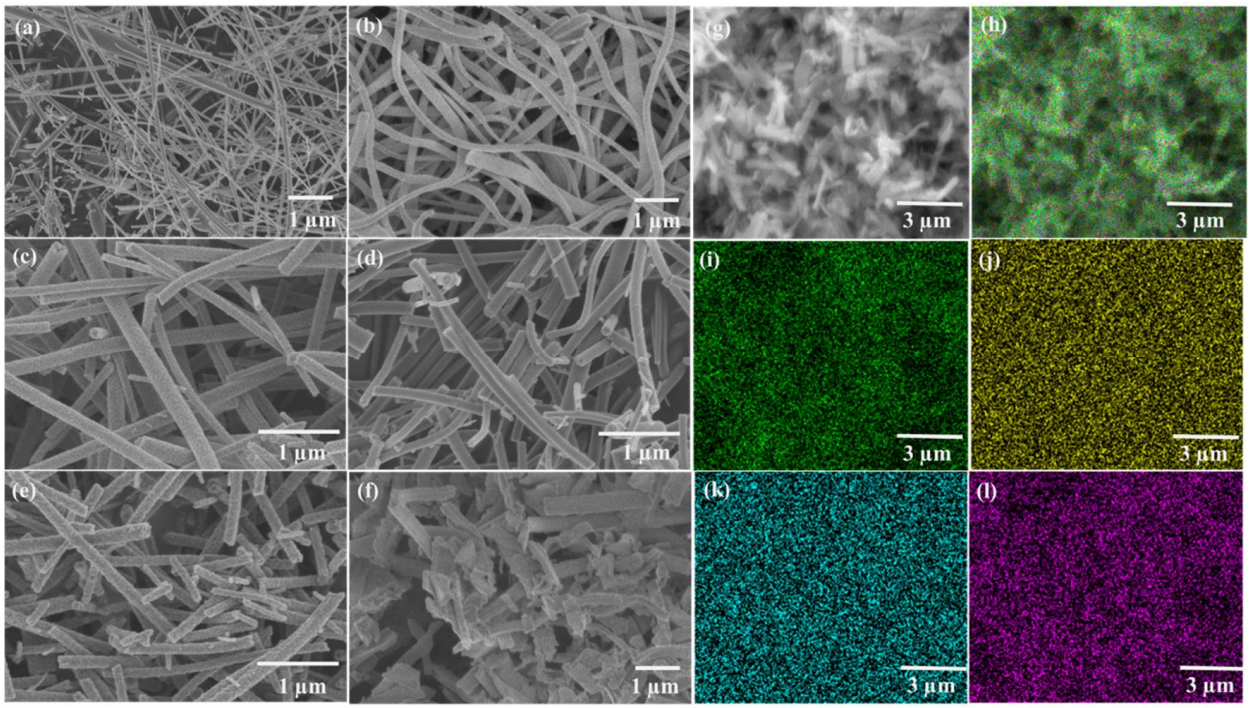

Figure 3. SEM images for (**a**) TW0, (**b**) TW10, (**c**) TW20, (**d**) TW30, (**e**) TW40 and (**f**) TW50 nanofibers; (**g**,**h**) Images of SEM/EDX elemental mapping of TW40 (**i**) oxygen, (**j**) titanium, (**k**) tungsten and (**l**) sulfur in TW40.

The optical characteristics of the fabricated nanofibers were determined using UV-Vis diffuse reflectance (UVDR), as presented in Figure 4. The UVDR–spectra of the nanofibers were examined in the range of 200–800 nm using UV-Vis optical spectroscopy. The optical band gaps (Eg) were obtained by the following equation:

$$\alpha h\nu = A(h\nu - Eg)^{(n/2)} \quad (1)$$

where α is the absorption coefficient, v is the frequency of light and n is the constant of proportionality (n equals 4 for the indirect transition in the prepared nanofibers) [20–22].

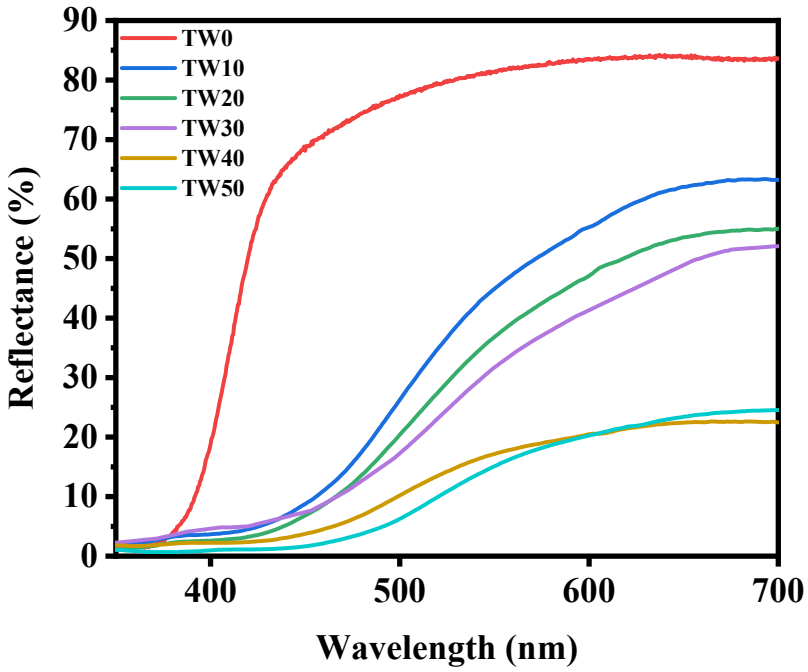

Figure 4. UV-Vis diffuse reflectance spectra of TW0, TW10, TW20, TW30, TW40 and TW50 nanofibers.

The prepared nanofibers had a red shift due to joining of WS_2 with TiO_2. As per the following sequence: 3.18, 2.87, 2.72, 2.68, 2.57 and 2.45 eV for TW0, TW10, TW20, TW30, TW40 and TW50, respectively. This recorded shift was due to the conjugation between WS_2 and TiO_2, also this conjugation was detected in the Raman and FTIR [14]. The TW40 sample has reflectance lower than other nanofibers due to the high absorption of light. In contrast, TW50 had a greater amount of WS_2, which led to the aggregation of WS_2 and reduced light absorbed, as seen in the SEM image.

2.2. Photocatalytic Degradation of Phenol under Visible Light by TWx Nanofibers

The adsorption test was evaluated in the dark for 1 h before illumination. Then the photocatalytic activity of phenol degradation was detected every hour during 4 h. The photodegradation of phenol reached 13, 47, 57, 74, 83 and 66% for TW0, TW10, TW20, TW30, TW40 and TW50, respectively, as presented in Figure 5a. The TW0 sample (TiO_2 nanofibers) provided low activity for photodegradation of phenol ~13% due to large band gap of 3.18 eV. In contrast, the combination of WS_2 with TiO_2 enhanced the catalytic activity of phenol degradation, reaching 83% for TW40. This can be attributed to the band gap decrease followed by active absorption of visible light, as obtained by UV-Vis diffuse reflectance spectra. In addition, the photocatalytic active sites were increased by the incorporation of 1D WS_2 with 2D TiO_2 nanofibers. The kinetic of phenol photodegradation by prepared nanofibers is presented in Figure 5b. The phenol degradation follows the first-order kinetics model of Langmuir−Hinshelwood which is presented in Equation (3) [23]. The apparent order rate constant (k) for TW0, TW10, TW20, TW30, TW40 and TW50 is 2.235×10^{-4}, 0.0017, 0.0024, 0.0043, 0.0057 and 0.0028 min^{-1}, respectively. Rate constants grow in this order: TW40 > TW30 > TW50 > TW20 > TW10 > TW0. The TW40 sample has the maximum rate constant (0.0057) that is attributed to the high interaction between WS_2 and TiO_2, as presented in SEM and Raman, besides the synergistic effect between WS_2 and TiO_2 nanofibers. In order to determine the role of hydroxyl radicals ($^{\bullet}OH$), holes (h^+) and superoxide anions ($^{\bullet}O^{2-}$) in the efficiency of photodegradation of phenol, we used different free radical trapping agents with TW40 nanofibers, as presented in Figure 5c. The scavengers were Tert-butyl alcohol (TBA), disodium ethylenediaminetetraacetic acid (Na_2-EDTA) and

p-benzoquinone (BQ) to trap free radicals of hydroxyl radicals ($^{\bullet}OH$), holes (h^{+}) and superoxide radicals ($^{\bullet}O^{2-}$), respectively [24,25]. The photodegradation of phenol varied according to different sacrificial agents. Predominantly, the photocatalytic degradation in presence of the TBA (5 mM) reduced to 36%. Therefore, the photogenerated $^{\bullet}OH$ radical is the important free radical component during the phenol photodegradation process [24,25]. Moreover, TW40 has high photodegradation stability up to five cycles, as presented in Figure 5d. The phenol photodegradation remained at the level of 80% after 5 cycles. The results obtained for the TW40 sample indicate a high photocatalytic degradation of phenol with a narrow bandgap, as well as an excellent stability of photocatalytic activity. We can note also that the crystallinity of TW40 nanofibers (Figure S1) and the morphology (Figure S2) were stable after five cycles as confirmed by XRD and SEM, respectively.

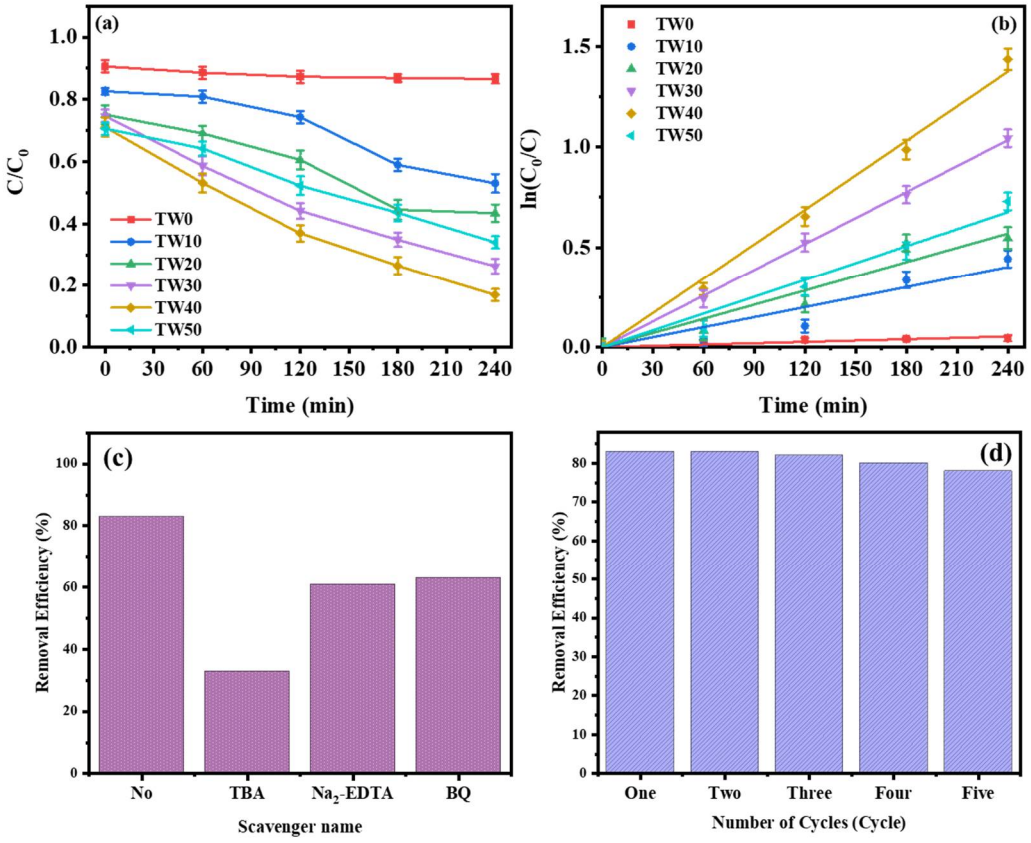

Figure 5. (**a**) Photocatalytic degradation of phenol for prepared nanofibers under visible light irradiation; (**b**) the ln(C/C0) changing versus time during visible light irradiation for prepared nanofibers; (**c**) Trapping test of the photogenerated free radicals and holes with TW40 nanofibers; (**d**) The stability cycles of phenol photodegradation using TW40 nanofibers under visible light irradiation for 4 h.

3. Materials and Methods

3.1. Chemical

Titanium (IV) isopropoxide 97%, WS2 powder, n-butyl lithium solution, hexane, absolute ethanol (99%), acetic acid (98%), polyvinylpyrrolidone (PVP; Mw = 1,300,000 g/mol) and phenol were purchased from Sigma Aldrich (St. Louis, MO, USA). All purchased compounds were used as received, without further purification.

3.2. Preparation of WS_2/TiO_2 Nanofibers

Tungsten disulfide (WS_2) with TiO_2 nanofibers was prepared using the electrospinning technique by different ratio between WS_2 and TiO_2. First, the solution (a) was prepared by 0.3 g of PVP dissolved in 3 mL of ethanol and 2 mL of acetic acid while stirring for 30 min,

then 1.5 mL of TTIP was added with stirring for 30 min. The solution (b) was prepared with different weight ratios of WS_2 in 2 mL of ethanol and sonicated for 2 h to obtain (TW0, TW10, TW20, TW30, TW40 and TW50 for TiO_2: WS_2 is 1:0, 0.9:0.1, 0.8:0.2, 0.7:0.3, 0.6:0.4 and 0.5:0.5, respectively). After that, solution (b) was mixed to solution (a) with stirring for 30 min. The solution was added in syringe with a stainless-steel nozzle with a diameter of 0.7 mm under flow rate 1 mL/h and voltage power (1.5 kV/cm) between the nozzle and the rotating collector. The collected nanofibers were calcined at 400 °C for 3 h.

3.3. Characterization

The nanofiber vibrational properties were observed using a dispersive Raman microscope with a laser wavelength of 532 nm and a power of 10 mW (Senterra, Bruker, Bremen, Germany). The functional groups of the prepared composite nanofibers were recognized using FTIR spectrometer (Perkin Elmer, Waltham, MA, USA) with the use of standard KBr pellet technique. The surface area of the nanofibers was detected from nitrogen adsorption–desorption isotherms at liquid nitrogen temperature using Micromeritics ASAP 2010 equipment (degassing conditions: 200 °C/12 h). The titanium and tungsten elemental concentrations in the as-prepared nanofibers were determined using atomic absorption spectroscopy (AAS) (Analyst 400, PerkinElmer, Bremen, Germany). The morphology of nanofibers was detected by SEM (Quanta-250 FEG, FEI, Netherlands) methods. The UV-Vis–DR spectra were measured by a Jasco V-570 (Jasco Inc., Easton, MD, USA).

3.4. Photocatalytic Activity Measurement

The photocatalytic activity of the WS_2/TiO_2 nanofibers was detected by tracing the photodegradation of phenol. The photocatalyst efficiency was detected by analyzing the decrease of phenol concentration during exposure to visible light radiation. The reaction temperature was fixed at 25 ± 0.2 °C by circulating water over the photoreactor. The photocatalytic performance was detected by using 10 mg of photocatalyst in 200 mL of phenol solution (50 ppm) under a 500 W linear halogen lamp (visible light radiation). The solution mixture was stirred in the dark for 1 h to obtain the adsorption/desorption equilibrium of phenol [26]. Then, the mixture was exposed to visible light for 4 h. Following, the sample was collected from reactor every 1 h and the catalyst was eliminated by a centrifuge to detect the organic pollutants' concentration in the solution by high-performance liquid chromatography (HPLC) equipped with a photodiode array detector (Agilent 1200 series, Agilent, Colorado Springs, CO, USA).

The degradation efficiency was measured by the following equation:

$$\text{degradation efficiency } \% = (((C_0 - C))/(C_0)) * 100 \quad (2)$$

where C_0 and C are the initial and final phenol concentration, respectively [27].

The kinetics of phenol photocatalytic degradation were calculated as follows (where k (min^{-1}) is the apparent rate constant):

$$\ln (C_t/C_0) = -kt \quad (3)$$

4. Conclusions

In brief, we have successfully prepared WS_2/TiO_2 nanofibers with different ratios between WS_2 (1D) and TiO_2 (2D). Structural and morphological analyses of the prepared nanofibers confirmed the incorporation between WS_2 and TiO_2. Significantly, the photocatalytic efficiency of TW40 for phenol degradation was as high as 83%. The remarkable photocatalytic performance of TW40 (1D/2D structure) was attributed to the synergism effect between WS_2 and TiO_2 to improve electron transfer. In addition, the linkage between WS_2 and TiO_2 enhanced the photocatalytic stability of the nanofibers. The trapping test for the photogenerated free radicals and holes of TW40 demonstrated that the photogenerated hydroxyl radicals ($^{\bullet}OH$) have a significant role in the photodegradation of phenol

as an organic pollutant. Therefore, WS_2/TiO_2 nanofibers act as promising materials for photo-degradation of organic pollutants in water.

Supplementary Materials: The following supporting information can be downloaded at: https://www.mdpi.com/article/10.3390/inorganics10040054/s1, Figure S1: XRD of TW40 nanofibers before and after photocatalytic reaction.; Figure S2: SEM of TW40 nanofibers after photocatalytic reaction.

Author Contributions: Study design, A.A.N.; methods, E.A.N. and H.H.E.-M.; validation, A.A.N., H.H.E.-M., Y.M.M., H.R.A., S.A.E.-W. and D.Y.S.; formal analysis, E.A.N., A.A.N. and H.H.E.-M.; performed experiments, E.A.N. and A.A.N.; data analysis, E.A.N., A.A.N. and H.H.E.-M.; original draft preparation, E.A.N. and A.A.N.; review and editing of the manuscript, E.A.N., H.H.E.-M., Y.M.M., H.R.A., S.A.E.-W., D.Y.S., P.R. and A.A.N.; study supervision, A.A.N., Y.M.M., P.R., H.H.E.-M. and S.A.E.-W.; project administration, A.A.N.; funding acquisition, A.A.N. All authors have read and agreed to the published version of the manuscript.

Funding: This research received no external funding.

Conflicts of Interest: The authors declare no conflict of interest.

References

1. Wang, G.; Huang, Y.; Li, G.; Zhang, H.; Wang, Y.; Li, B.; Wang, J.; Song, Y. Preparation of a novel sonocatalyst, Au/$NiGa_2O_4$-Au-Bi_2O_3 nanocomposite, and application in sonocatalytic degradation of organic pollutants. *Ultrason. Sonochem.* **2017**, *38*, 335–346. [CrossRef] [PubMed]
2. Manavi, N.; Kazemi, A.S.; Bonakdarpour, B. The development of aerobic granules from conventional activated sludge under anaerobic-aerobic cycles and their adaptation for treatment of dyeing wastewater. *Chem. Eng. J.* **2017**, *312*, 375–384. [CrossRef]
3. El-Maghrabi, H.H.; Al-Kahlawy, A.A.; Nada, A.A.; Zaki, T. Photocorrosion resistant Ag_2CO_3@Fe_2O_3/TiO_2-NT nanocomposite for efficient visible light photocatalytic degradation activities. *J. Hazard. Mater.* **2018**, *360*, 250–256. [CrossRef] [PubMed]
4. Pant, B.; Ojha, G.P.; Kuk, Y.-S.; Kwon, O.H.; Park, Y.W.; Park, M. Synthesis and Characterization of ZnO-TiO_2/Carbon Fiber Composite with Enhanced Photocatalytic Properties. *Nanomaterials* **2020**, *10*, 1960. [CrossRef] [PubMed]
5. Chandrabose, G.; Dey, A.; Gaur, S.S.; Pitchaimuthu, S.; Jagadeesan, H.; Braithwaite, N.S.J.; Selvaraj, V.; Kumar, V.; Krishnamurthy, S. Removal and degradation of mixed dye pollutants by integrated adsorption-photocatalysis technique using 2-D MoS_2/TiO_2 nanocomposite. *Chemosphere* **2021**, *279*, 130467. [CrossRef]
6. Boningari, T.; Inturi, S.N.R.; Suidan, M.; Smirniotis, P.G. Novel one-step synthesis of nitrogen-doped TiO_2 by flame aerosol technique for visible-light photocatalysis: Effect of synthesis parameters and secondary nitrogen (N) source. *Chem. Eng. J.* **2018**, *350*, 324–334. [CrossRef]
7. Chen, J.; Shan, M.; Shi, X.; Zhang, S.; Li, J.; Luan, J.; Duan, L.; Hou, H. $BiSnSbO_6$–TiO_2 composites enhance LED light-driven photocatalytic antibacterial activity. *Ceram. Int.* **2022**, *in press*. [CrossRef]
8. Nur, A.S.M.; Sultana, M.; Mondal, A.; Islam, S.; Robel, F.N.; Islam, A.; Sumi, M.S.A. A review on the development of elemental and codoped TiO_2 photocatalysts for enhanced dye degradation under UV–vis irradiation. *J. Water Process Eng.* **2022**, *47*, 102728. [CrossRef]
9. Nada, A.A.; el Rouby, W.M.A.; Bekheet, M.F.; Antuch, M.; Weber, M.; Miele, P.; Viter, R.; Roualdes, S.; Millet, P.; Bechelany, M. Highly textured boron/nitrogen co-doped TiO_2 with honeycomb structure showing enhanced visible-light photoelectrocatalytic activity. *Appl. Surf. Sci.* **2020**, *505*, 144419. [CrossRef]
10. Kawrani, S.; Boulos, M.; Bekheet, M.F.; Viter, R.; Nada, A.A.; Riedel, W.; Roualdes, S.; Cornu, D.; Bechelany, M. Segregation of copper oxide on calcium copper titanate surface induced by Graphene Oxide for Water splitting applications. *Appl. Surf. Sci.* **2020**, *516*, 146051. [CrossRef]
11. Nada, A.A.; Bekheet, M.F.; Roualdes, S.; Gurlo, A.; Ayral, A. Functionalization of MCM-41 with titanium oxynitride deposited via PECVD for enhanced removal of methylene blue. *J. Mol. Liq.* **2019**, *274*, 505–515. [CrossRef]
12. Yuan, J.; Najmaei, S.; Zhang, Z.; Zhang, J.; Lei, S.; Ajayan, P.M.; Yakobson, B.I.; Lou, J. Photoluminescence quenching and charge transfer in artificial heterostacks of monolayer transition metal dichalcogenides and few-layer black phosphorus. *ACS Nano* **2015**, *9*, 555–563. [CrossRef] [PubMed]
13. Zhao, X.; Ma, X.; Sun, J.; Li, D.; Yang, X. Enhanced catalytic activities of surfactant-assisted exfoliated WS2 nanodots for hydrogen evolution. *ACS Nano* **2016**, *10*, 2159–2166. [CrossRef] [PubMed]
14. Voiry, D.; Yamaguchi, H.; Li, J.; Silva, R.; Alves, D.C.B.; Fujita, T.; Chen, M.; Asefa, T.; Shenoy, V.B.; Eda, G. Enhanced catalytic activity in strained chemically exfoliated WS_2 nanosheets for hydrogen evolution. *Nat. Mater.* **2013**, *12*, 850–855. [CrossRef]
15. Elías, A.L.; Perea-López, N.; Castro-Beltrán, A.; Berkdemir, A.; Lv, R.; Feng, S.; Long, A.D.; Hayashi, T.; Kim, Y.A.; Endo, M. Controlled synthesis and transfer of large-area WS_2 sheets: From single layer to few layers. *ACS Nano* **2013**, *7*, 5235–5242. [CrossRef]
16. Xiang, Q.; Yu, J.; Jaroniec, M. Synergetic effect of MoS_2 and graphene as cocatalysts for enhanced photocatalytic H_2 production activity of TiO_2 nanoparticles. *J. Am. Chem. Soc.* **2012**, *134*, 6575–6578. [CrossRef]

17. Golovnev, N.N.; Molokeev, M.S.; Vereshchagin, S.N.; Atuchin, V.V. Calcium and strontium thiobarbiturates with discrete and polymeric structures. *J. Coord. Chem.* **2013**, *66*, 4119–4130. [CrossRef]
18. Smitha, V.S.; Manjumol, K.A.; Baiju, K.V.; Ghosh, S.; Perumal, P.; Warrier, K.G.K. Sol–gel route to synthesize titania-silica nano precursors for photoactive particulates and coatings. *J. Sol-Gel Sci. Technol.* **2010**, *54*, 203–211. [CrossRef]
19. Golovnev, N.N.; Solovyov, L.A.; Lesnikov, M.K.; Vereshchagin, S.N.; Atuchin, V.V. Hydrated and anhydrous cobalt (II) barbiturates: Crystal structures, spectroscopic and thermal properties. *Inorg. Chim. Acta* **2017**, *467*, 39–45. [CrossRef]
20. Atuchin, V.V.; Isaenko, L.I.; Kesler, V.G.; Lin, Z.S.; Molokeev, M.S.; Yelisseyev, A.P.; Zhurkov, S.A. Exploration on anion ordering, optical properties and electronic structure in $K_3WO_3F_3$ elpasolite. *J. Solid State Chem.* **2012**, *187*, 159–164. [CrossRef]
21. Ji, H.; Huang, Z.; Xia, Z.; Molokeev, M.S.; Jiang, X.; Lin, Z.; Atuchin, V.V. Comparative investigations of the crystal structure and photoluminescence property of eulytite-type $Ba_3Eu(PO_4)_3$ and $Sr_3Eu(PO_4)_3$. *Dalton Trans.* **2015**, *44*, 7679–7686. [CrossRef] [PubMed]
22. Atuchin, V.V.; Subanakov, A.K.; Aleksandrovsky, A.S.; Bazarov, B.G.; Bazarova, J.G.; Dorzhieva, S.G.; Gavrilova, T.A.; Krylov, A.S.; Molokeev, M.S.; Oreshonkov, A.S. Exploration of structural, thermal, vibrational and spectroscopic properties of new noncentrosymmetric double borate $Rb_3NdB_6O_{12}$. *Adv. Powder Technol.* **2017**, *28*, 1309–1315. [CrossRef]
23. Elshypany, R.; Selim, H.; Zakaria, K.; Moustafa, A.H.; Sadeek, S.A.; Sharaa, S.I.; Raynaud, P.; Nada, A.A. Magnetic ZnO Crystal Nanoparticle Growth on Reduced Graphene Oxide for Enhanced Photocatalytic Performance under Visible Light Irradiation. *Molecules* **2021**, *26*, 2269. [CrossRef] [PubMed]
24. Elshypany, R.; Selim, H.; Zakaria, K.; Moustafa, A.H.; Sadeek, S.A.; Sharaa, S.I.; Raynaud, P.; Nada, A.A. Elaboration of Fe_3O_4/ZnO nanocomposite with highly performance photocatalytic activity for degradation methylene blue under visible light irradiation. *Environ. Technol. Innov.* **2021**, *23*, 101710. [CrossRef]
25. Nada, A.A.; Orimolade, B.O.; El-Maghrabi, H.H.; Koiki, B.A.; Rivallin, M.; Bekheet, M.F.; Viter, R.; Damberga, D.; Lesage, G.; Iatsunskyi, I. Photoelectrocatalysis of paracetamol on Pd–ZnO/N-doped carbon nanofibers electrode. *Appl. Mater. Today* **2021**, *24*, 101129. [CrossRef]
26. Nasr, M.; Balme, S.; Eid, C.; Habchi, R.; Miele, P.; Bechelany, M. Enhanced visible-light photocatalytic performance of electrospun rGO/TiO_2 composite nanofibers. *J. Phys. Chem. C* **2017**, *121*, 261–269. [CrossRef]
27. Sugi, S.; Rajalakshmi, P.U.; Shanthi, J. Photocatalytic Degradation efficiency of CuXZn1-XO Composite. *Optik* **2017**, *131*, 406–413. [CrossRef]